Peng, X., and Zornberg, J.G. (2017). "Evaluation of Load Transfer in Geogrids for Base Stabilization using Transparent Soil." Procedia Engineering, Elsevier, Transportation Geotechnics and Geoecology, May, Vol. 189, pp. 307-314.

Available online at www.sciencedirect.com

ScienceDirect

Procedia Engineering 189 (2017) 307 – 314

Procedia Engineering

www.elsevier.com/locate/procedia

Transportation Geotechnics and Geoecology, TGG 2017, 17-19 May 2017, Saint Petersburg, Russia

Evaluation of load transfer in geogrids for base stabilization using transparent soil

Xin Peng[a], Jorge G. Zornberg[a] *

[a]*Department of Civil, Architectural and Environmental Engineering, the University of Texas at Austin, 301 E. Dean Keeton St. Stop C1700, Austin, Texas, 78712-0273, USA*

Abstract

The design of roadways with geosynthetic-stabilized base layers requires proper evaluation of the load-transfer mechanisms between soil particles and geosynthetics. In the case of geogrid reinforcements, the resistances mobilized on rib elements are key factors that determine the mechanical responses for both: (1) the ultimate pullout strength; and (2) the in-plane stiffness. Geogrids with different aperture shapes have rib elements along different orientations, and different rib orientations could generate different load transfer mechanisms. In this study, a new experimental testing program using transparent soil was conducted to visualize the load transfer of geogrids with different aperture shapes (e.g. rectangular, triangular). Specifically, small-scale soil-geosynthetic interaction tests were conducted using high-definition cameras. Consequently, image-processing techniques were used to obtain the displacements and deformations of geogrid specimens from digital images. The soil-geogrid interaction behaviors for geogrid specimens with different aperture shapes were evaluated and compared. Overall, multiple mechanisms for load transfer between soil and geogrids with different geometric characteristics could be characterized and quantified using new techniques involving transparent soil and digital image analysis.

Peer-review under responsibility of the scientific committee of the International conference on Transportation Geotechnics and Geoecology

Keywords: geosynthetics; geogrid; transparent soil; stabilization; load transfer; image analysis

* Corresponding author. Tel.: +1-512-232-3595; fax: +1-512-471-6548.
E-mail address: zornberg@mail.utexas.edu

Peer-review under responsibility of the scientific committee of the International conference on Transportation Geotechnics and Geoecology
doi:10.1016/j.proeng.2017.05.049

1. Introduction

The use of different types of geogrids in the design of reinforced soil retaining structures and stabilized roadways requires proper evaluation of the load transfer mechanisms between soil and reinforcement. A number of experimental [1,2,3,4,5] and numerical [5,6,7] studies investigating these mechanisms were conducted over the past decades. Based on these studies, the resistance mobilized on the geogrid specimen is typically considered to result from two contributions: (1) resistance generated from longitudinal ribs; and (2) passive resistance developed at the frontal surface of the transverse ribs. In the application of pavement stabilization, the improved stiffness behaviors of geogrid-stabilized base layers were evaluated via laboratory and field tests [8,9,10]. However, the load transfer mechanisms between soil particles and geogrid elements is still not fully understood to explain the increased stiffness performance of the soil-geogrid composite layer.

Transparent soils, such as those containing amorphous silica materials, and pore fluids with a matching refractive index have recently been utilized in typical geotechnical studies to measure continuous spatial deformations in soils. Iskander [11], Ezzein and Bathurst [12] introduced several types of transparent soils, and documented their geotechnical properties and optical measurement methods. Ezzein and Bathurst [13] used a large-scale pullout test apparatus with transparent granular soil to evaluate the mobilization of the geogrid joints' displacement at different pullout load levels. Ferreira and Zornberg [14] conducted small-scale pullout tests with transparent granular soil and geogrids with markers to track geogrid displacements as well as the movement of soil particles during pullout loading.

Uniaxial and biaxial geogrids have been widely utilized to stabilize roadways. In recent years, geogrids with triangular apertures have been introduced into the market for their potential geometric advantages, as compared to traditional uniaxial and biaxial geogrids. These include: (1) offering three principal directions of stiffness instead of one or two; (2) comparatively larger rib depth to facilitate confinement of soil particles; and (3) a hexagonal junction shape with comparatively high junction strength and stiffness. Dong et al. [15] conducted numerical evaluations to compare the tensile behavior of geogrids with rectangular apertures against that of geogrids with triangular apertures. They concluded that under tensile loading triaxial geogrids have far more uniform stress and strain distributions than geogrids with rectangular apertures. Sun et al. [16] indicated that in comparison to unstabilized sections, triaxial geogrid-stabilized pavement sections exhibited reductions in surface and subgrade permanent deformations, as well as a reduction in the horizontal pressures within the subgrade.

2. Materials and methods

2.1. Transparent granular soil

The solid material used in this study was crushed fused quartz. According to the Unified Soil Classification System (USCS) the particle size range of this material is poorly graded sand (SP). Some basic geotechnical properties measured according to ASTM standards are summarized in **Ошибка! Источник ссылки не найден.**

Table 1. Geotechnical properties of crushed fused quartz.

Property	Test method	Value
Specific gravity (20°C)	Water Pycnometer Test (ASTM D854)	2.203
Maximum–index dry density (g/cm3)	Vibratory Table Test (ASTM D4253)	1.336
Minimum–index dry density (g/cm3)	Vibratory Table Test (ASTM D4254)	1.203
Friction angle, dry (o)	Direct Shear Test (ASTM D3080)	45
Friction angle, oil saturated, drained (o)	Direct Shear Test (ASTM D3080)	44

The pore fluid used with the transparent soil contained a mixture of two clear mineral oils: Puretol 7 and Paraflex HT4. Puretol 7 has a higher refractive index (RI) than the solid fused quartz (RI: 1.4585), while Paraflex HT4 has a lower refractive index. Therefore, for the given volume ratio of these two liquids, the final combination aimed at

having the same refractive index as that of fused quartz. Based on the direct shear tests shown in **Ошибка! Источник ссылки не найден.**, due to the potential lubrication of the pore fluid, the friction angle of the oil-saturated soil is one degree less than that of the dry particles. A transparent soil sample (approximately 2/3 of the fused quartz from the bottom was fully saturated with the oil mixture and the top 1/3 of the fused quartz was in a dry condition) with an inserted biaxial geogrid is displayed in Fig. 1.

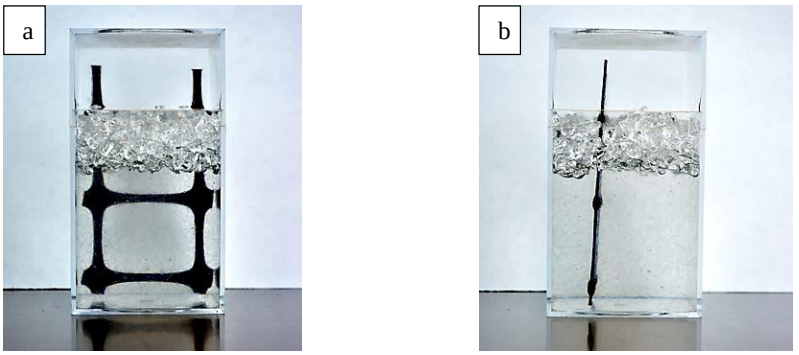

Fig. 1. (a) Frontal view and (b) side view of a transparent soil sample and inserted biaxial geogrid.

2.2. Geogrid type

The geogrids used in this study were manufactured by punching out holes in polypropylene sheets, and then heating and stretching them along different directions. To evaluate and compare load transfer mechanisms between soil particles and different geogrids, two geogrid types – one with rectangular and one with triangular aperture shapes – were used in experimental tests. The nominal geometric characteristics of both geogrids are presented in Table 2. For G2 (with triangular apertures), all ribs are oriented in three substantially equilateral directions.

Table 2. Geometric properties of the geogrids used in this study (from manufacturer's specification sheet).

Geogrid	Aperture shape	Rib	Rib pitch (mm)	Mid-rib depth (mm)	Mid-rib width (mm)
G1	Rectangular	Longitudinal	25	0.76	3.0
		Transverse	33		3.0
G2	Triangular	Longitudinal	40	1.6	1.3
		Diagonal		2.0	1.0

2.3. Small-scale soil-geosynthetic interaction test setup

Fig. 2 illustrates the test apparatus used in this study. The loading system and data acquisition system were the same as those reported by Ferreira [17]. A high-definition camera was used to capture deformations of the entire geogrid in the confined portion of the sample. The sampling rate was 5 seconds, and a loading displacement rate of 1 mm/min was applied during testing. Frontal unit tension and captured images were synchronized by the data acquisition system. A light system, composed of two 160 W photo studio soft boxes, was used to provide uniform light on the transparent pullout box. The internal dimensions of the transparent box were 300 mm × 250 mm × 150 mm (width × length × height), and the dimensions of the confined portion of the triaxial geogrid were about 210 mm × 230 mm (width × length).

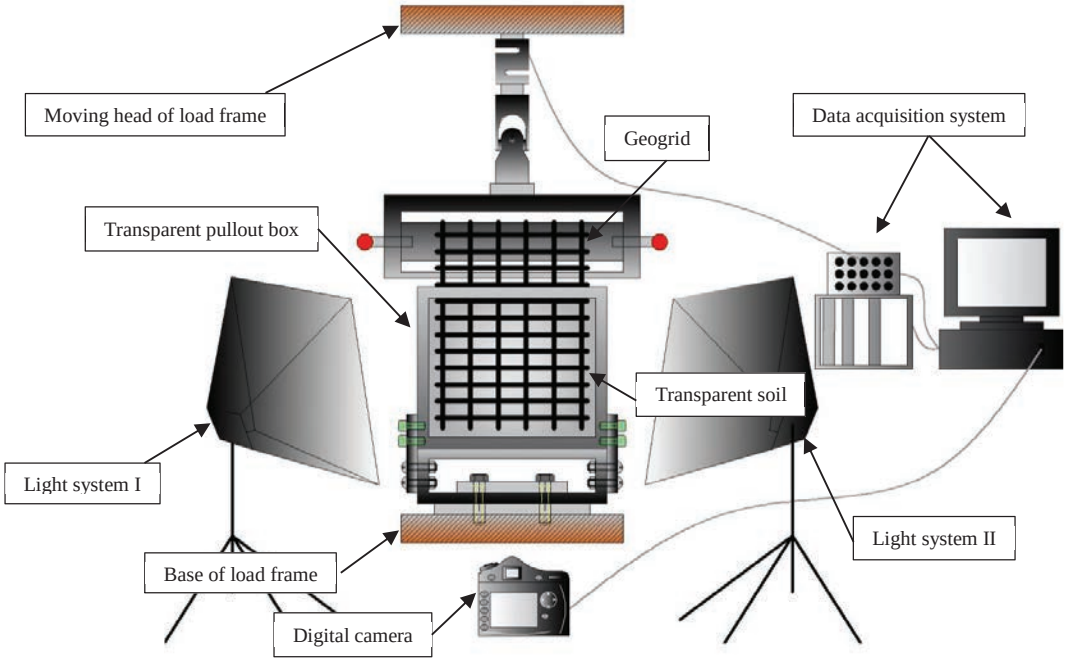

Fig. 2. Soil-geosynthetic interaction test setup with transparent soil.

2.4. Image processing techniques

Greyscale images captured during testing were used to track deformations of the geogrid. An open source image processing tool package – ImageJ – was utilized for some basic image processing, and further deformation capturing and data analysis were conducted using Matlab programing codes. Oil- and friction-resistant white markers were used to track displacements and deformations of G1(a). The Digital Image Correlation (DIC) technique was used to observe the displacements of the rib junctions and deformations of ribs (Fig. 3b).

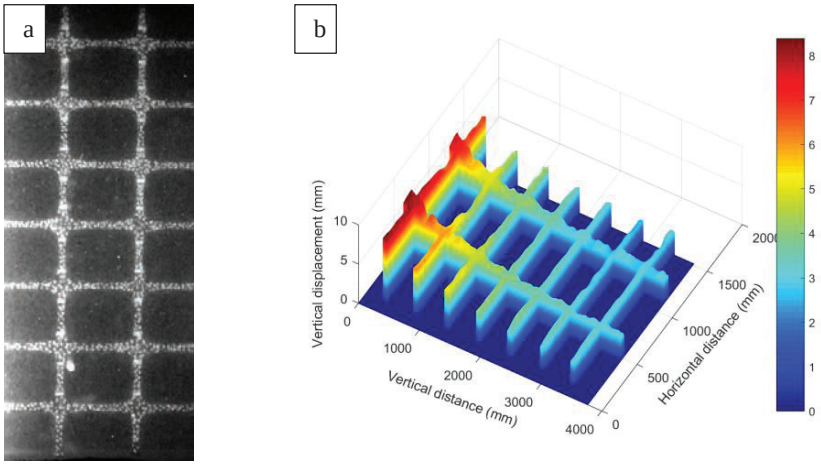

Fig. 3. (a) Frontal view of the center section of undeformed G1 in the transparent pullout box with transparent soil and (b) displacement field of this section of deformed G1 along pullout direction from DIC analysis.

3. Test Results and Discussion

Results from tests using transparent soil with geogrids G1 and G2 are presented in this section. Tests were conducted using an applied normal pressure of 27.6 kN/m^2 at a constant displacement rate of 1 mm/min.

DIC codes were used to track the junction displacement for G1 and G2. Junction displacement profiles along the pullout direction for G1 and G2 at different frontal unit tensions are shown in Fig. 4.

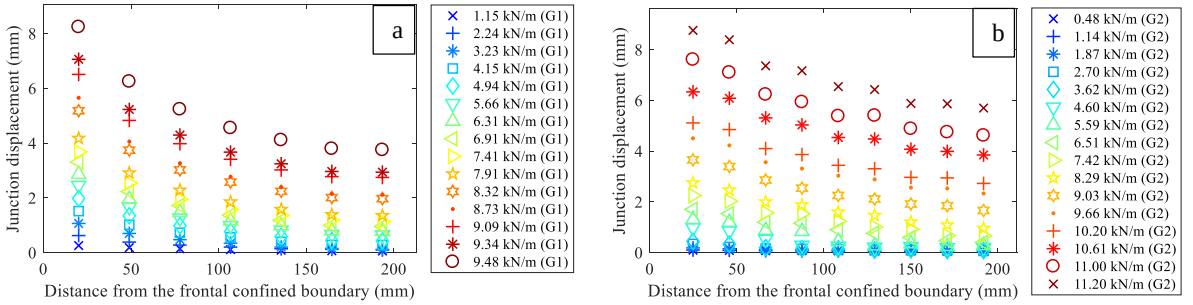

Fig. 4. Junction displacement profiles along the pullout direction for (a) G1 and (b) G2 at different levels of frontal unit tension.

Junction displacement profiles for G1 and G2 at similar frontal unit tensions along the pullout direction are compared in Fig. 5. Two main observations can be made based on Fig. 5: (1) for each of the four plots, even though the frontal unit tension of G2 was slightly higher than G1, all G2 junctions still had fewer displacements along the pullout direction than G1; (2) for the given frontal unit tensions, G1 generally had steeper and more curved junction displacement profiles than G2. The tangent slopes of the displacement profiles are strains at corresponding locations. Fig. 5 also illustrates that G2 typically had fewer strains (slopes) in at least the first half of the specimen length from the frontal confined boundary as compared to G1, and had significantly fewer changes in strains (changes in slopes) along the specimen's entire embedment length. More uniform strains along G2 could be explained as a more uniform load distribution generated on the specimen.

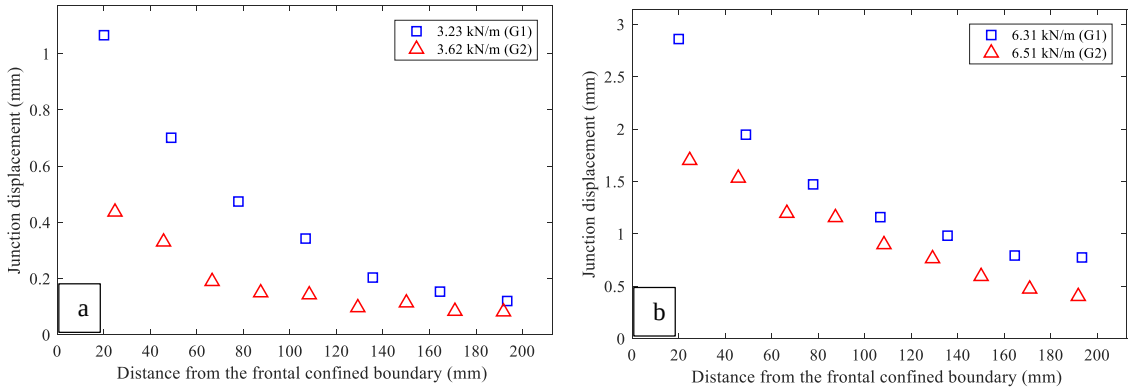

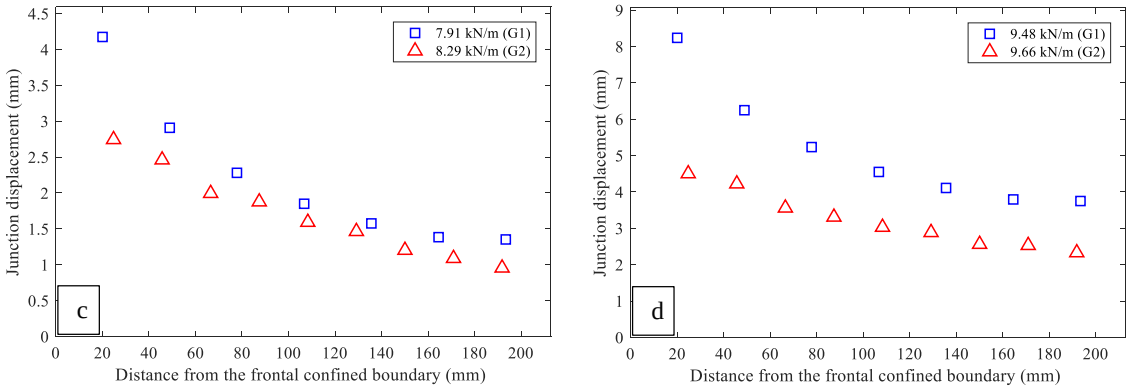

Fig. 5. Comparisons of junction displacement profiles between G1 and G2 at different levels of frontal unit tension.

For a comparison of the confined stiffness performance between G1 and G2, junctions at the front, middle and end locations of the geogrid specimens were selected. The distances from the frontal confined boundary to these three junction locations are tabulated in Table 3. Comparisons of the relationships between frontal unit tension and junction displacement at these three locations are plotted in Fig. 6.

Table 3. Junction locations of G1 and G2 for the comparison of confined stiffness performance.

Geogrid	Distance from the frontal confined boundary to junction at Location A (mm)	Distance from the frontal confined boundary to junction at Location B (mm)	Distance from the frontal confined boundary to junction at Location C (mm)
G1	49	107	193
G2	46	108	192

Fig. 6 shows that G2 consistently had fewer junction displacements for the given frontal unit tensions at all selected locations than G1, which indicates a better confined stiffness performance for G2. When examined together, results from Fig. 5 and Fig. 6 indicate a more uniform load transfer along the entire soil-geogrid interface for G2 than for G1, and relatively stiffer confined behaviors for G2 than for G1.

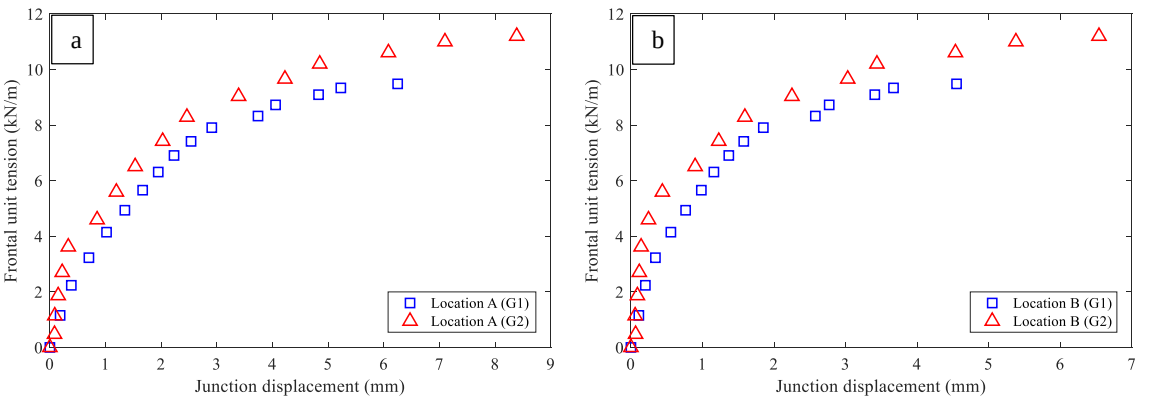

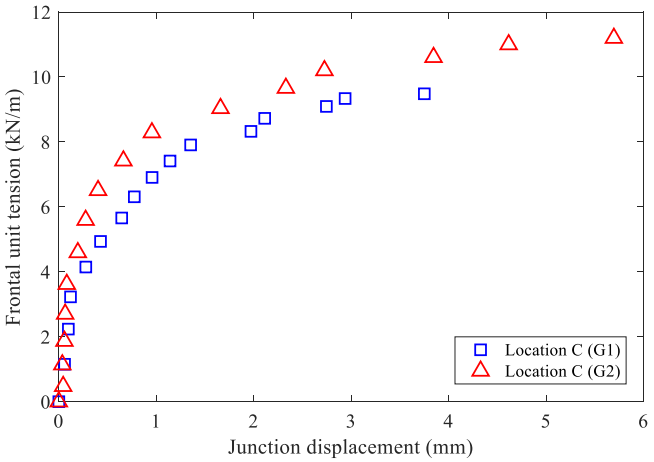

Fig. 6. Comparisons of confined stiffness performances between G1 and G2 at (a) Location A, (b) Location B and (c) Location C.

4. Conclusions

Load transfer mechanisms of geogrids with different aperture shapes and rib dimensions were evaluated using transparent soil and integrated image processing techniques. Based on results from small-scale soil-geosynthetic interaction tests, the following conclusions were drawn:

1) The use of transparent soil and image processing techniques adopted in this study were found to be adequate to capture displacements and deformations without creating physical disturbances at the soil-geosynthetic interface (as traditional sensor measurements typically have).
2) Junction displacement profiles along the pullout direction for G1 and G2 were compared at selected frontal unit tensions, and all G2 junctions exhibited fewer displacements than those for G1.
3) For the given frontal unit tensions, G1 generally had steeper and more curved junction displacement profiles than G2, which indicates that G1 generated larger strains and larger strain changes along the pullout direction than G2.
4) The confined stiffness performance between G1 and G2 at three different junction locations along the specimens were compared throughout testing. G2 consistently showed fewer displacements than G1 at those locations, regardless of frontal unit tension levels, which demonstrates that the confined stiffness behavior was generally better for G2 than G1.

Acknowledgements

The authors greatly appreciate Tensar International Corporation who provided the geogrids used in this study. The authors also gratefully acknowledge Dr. Julio Ferreira who finished the initial design of the soil-geosynthetic interaction test setup.

References

[1] H. Ochiai, J. Otani, S. Hayashic, T. Hirai, The pull-out resistance of geogrids in reinforced soil. Geotext Geomembr. 1996;14(1):19–42.
[2] A.M.N. Alagiyawanna, M. Sugimoto, S. Sato, H. Toyota, Influence of longitudinal and transverse members on geogrid pullout behavior during deformation. Geotext Geomembr. 2001;19(8):483–507.
[3] S.H. Teixeira, B.S. Bueno, J.G. Zornberg, Pullout resistance of individual longitudinal and transverse geogrid ribs. J Geotech Geoenvironmental Eng. 2007;133(1):37–50.

[4] A.C.C. Sieira, D.M. Gerscovich, A.S. Sayao, Displacement and load transfer mechanisms of geogrids under pullout condition. Geotext Geomembr. 2009;27(4):241–253.
[5] Z. Wang, F. Jacobs, M. Ziegler, Experimental and DEM investigation of geogrid–soil interaction under pullout loads. Geotext Geomembr. 2016 Jun;44(3):230–46.
[6] R.F. Wilson-Fahmy, R.M. Koerner, Finite element modelling of soil-geogrid interaction with application to the behavior of geogrids in a pullout loading condition. Geotext Geomembr. 1993;12(5):479–501.
[7] V.D.H. Tran, M.A. Meguid, L.E. Chouinard, A finite–discrete element framework for the 3D modeling of geogrid–soil interaction under pullout loading conditions. Geotext Geomembr. 2013;37:1–9.
[8] J.G. Collin, T.C. Kinney, X. Fu, Full scale highway load test of flexible pavement systems with geogrid reinforced base courses. Geosynth Int. 1996;3(4):537–549.
[9] Q. Chen, M. Abu-Farsakh, M. Tao, Laboratory evaluation of geogrid base reinforcement and corresponding instrumentation program. ASTM Geotech Test J. 2009;32(6):516–525.
[10] M.Y. Abu-Farsakh, Q. Chen, Evaluation of geogrid base reinforcement in flexible pavement using cyclic plate load testing. Int J Pavement Eng. 2011;12(3):275–288.
[11] M. Iskander, Modelling with transparent soils: Visualizing soil structure interaction and multi phase flow, non-intrusively. Springer Science & Business Media; 2010.
[12] F.M. Ezzein, R.J. Bathurst, A Transparent Sand for Geotechnical Laboratory Modeling. ASTM Geotech Test J. 2011;34(6):590–601.
[13] F.M. Ezzein, R.J. Bathurst, A new approach to evaluate soil-geosynthetic interaction using a novel pullout test apparatus and transparent granular soil. Geotext Geomembr. 2014;42(3):246–255.
[14] J.A. Ferreira, J.G. Zornberg, A Transparent Pullout Testing Device for 3D Evaluation of Soil–Geogrid Interaction. Geotech Test J. 2015;38(5):686–707.
[15] Y-L Dong, J. Han, X-H Bai, Numerical analysis of tensile behavior of geogrids with rectangular and triangular apertures. Geotext Geomembr. 2011;29(2):83–91.
[16] X. Sun, J. Han, M.H. Wayne, R.L. Parsons, J. Kwon, Experimental Study on Resilient Behavior of Triaxial Geogrid-Stabilized Unpaved Roads. In: Ground Improvement and Geosynthetics. ASCE; 2014. p. 353–362.
[17] J.A.Z. Ferreira, Evaluation of soil-geogrid interaction at different load levels using pullout tests and transparent soil (Doctoral dissertation). 2013. Available from: https://repositories.lib.utexas.edu/handle/2152/21153